ACS APPLIED MATERIALS & INTERFACES

Research Article

www.acsami.org

Zwitterionic Nanoparticles Constructed with Well-Defined Reduction-Responsive Shell and pH-Sensitive Core for "Spatiotemporally Pinpointed" Drug Delivery

Pingsheng Huang,[†,‡] Jinjian Liu,[§,‡] Weiwei Wang,[⊥] Chen Li,[⊥] Junhui Zhou,[†] Xue Wang,[†] Liandong Deng,[†] Deling Kong,[⊥] Jianfeng Liu,*[,§] and Anjie Dong*[,†]

[†]Department of Polymer Science and Technology, Key Laboratory of Systems Bioengineering of the Ministry of Education, Collaborative Innovation Center of Chemical Science and Engineering (Tianjin), School of Chemical Engineering and Technology, Tianjin University, Tianjin 300072, China

[§]Tianjin Key Laboratory of Molecular Nuclear Medicine, Institute of Radiation Medicine, and [⊥]Institute of Biomedical Engineering, Chinese Academy of Medical Science & Peking Union Medical College, Tianjin 300192, China

Supporting Information

ABSTRACT: Enabling nanocarriers to complete the sophisticated journey from the initial injection site to the targeted tumor cells and achieve "spatiotemporally pinpointed" drug release intracellularly is a challenging task in anticancer drug delivery. Herein, versatile shell-cross-linked nanoparticles (SCNPs) were prepared by one-step assembly of triblock zwitterionic copolymers, polycarboxybetaine methacrylate-*block*-poly(*N*-(2-(2-pyridyl disulde) ethyl methacrylamide-*block*-poly(2-(diisopropylamino) ethyl methacrylate) (PCB-*b*-PDS-*b*-PDPA, termed as PCSSD), which was well-defined via reversible additive fragment transfer (RAFT) polymerization, followed by functionalization with Arg-Gly-Asp (RGD). Thus, the RGD-PCSSD SCNPs cooperatively combine the ultra pH-sensitive PDPA core for efficient drug loading and pH-responsive drug release, the disulfide-cross-linked PDS shell that prevents premature drug release, the zwitterionic PCB corona to stabilize the SCNPs and prolong its systemic circulation, the RGD ligand for active tumor targeting and receptor-mediated endocytosis. Doxorubicin (DOX) was loaded as a model medicine (termed as RGD-PCSSD/DOX SCNPs). The dual-sensitivity studies showed that the pH-sensitivity of PDPA core could be adjusted by the shell-cross-linking density, accompanied by better control over premature drug release. Furthermore, results obtained by flow cytometry and fluorescence microscopy analysis demonstrated that once the RGD-PCSS$_{10}$D/DOX SCNPs were internalized into tumor cells via receptor-mediated endocytosis, boost drug release was observed with considerable cytotoxicity in vitro. The results of ex vivo imaging studies further confirmed the successful drug delivery from the injection site to the tumor tissue. In summary, the well-constructed RGD-PCSS$_{10}$D/DOX SCNPs with cooperative multifunctionality showed great potential as novel nanocarriers for tumor targeted anticancer drug delivery.

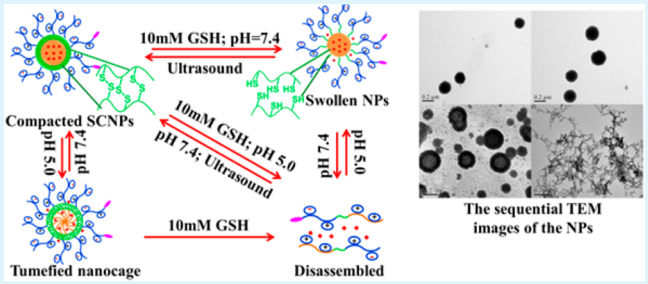

KEYWORDS: *pH-sensitive, shell-cross-linked, zwitterionic copolymer, tumor targeting, doxorubicin*

1. INTRODUCTION

The development of polymeric nanoparticles (NPs) assembled from amphiphilic copolymers for anticancer drug delivery is a burgeoning research area, chiefly because of its enhanced therapeutic benefits for cancer therapy.[1−3] However, this technique is facing tremendous challenges, because the drug-loaded NPs are subjected to multistages of systemic circulation, extravasation, accumulation, distribution, endocytosis, intracellular release, and drug action while circulating from the injection sites to the targeted tumor cells.[4] As a result, an effective NPs-based drug delivery system should be designed to exert its limitless versatility to maximize the drug delivery efficiency and therapeutic effect in view of all above stages.[5] In addition to fine control over the physicochemical properties, including composition, size, shape and surface chemistry to facilitate the accumulation of NPs at the tumor site, controlled-responsive drug release is also of paramount importance for improving the treatment efficiency.[6−9] As reported, traditional polymeric NPs usually show a "burst release" of up to 20−30% of the encapsulated drugs within the first few hours after injection, followed by diffusion-controlled release lasting for several days. This inevitably leads to drug loss in the systemic circulation and drug associated side effects due to unspecific drug actions.[10−12]

Hence, to endow the polymeric NPs with better controlled-release properties, the incorporation of cross-linking structures

Received: June 20, 2014
Accepted: August 6, 2014
Published: August 6, 2014

into NPs has emerged as a feasible strategy to minimize premature drug release.[13−15] Among various methods, the utilization of reversible disulfide-containing cross-linking is of particular interest, as it can be cleaved intracellularly by glutathione (GSH), which is a kind of reductases that can be found at 2−20 μM in the body fluids and normal extracellular matrices, and 2−10 mM in the cytosol and nuclei of tumor cells.[16,17] Shell-cross-linked NPs (SCNPs) have demonstrated great potential to inhibit premature drug leakage and facilitate drug release within tumor cells by disrupting the cross-linked structure, however, the drug release pattern of most SCNPs still follows a slow diffusion-controlled mechanism from the nonsensitive hydrophobic cores, leading to low drug bioavailability and insufficient cancer cell killing, resulting in potential multidrug resistance.[18,19]

On the other hand, to enhance the pinpointed intracellular drug release of polymeric NPs, different mechanisms have been incorporated according to the specific microenvironments of tumor cells, which are typically characterized by acidic pH within the endo/lysosomes, abundant enzymes in the lysosomes, and high redox potential in the cytosol and nuclei.[20,21] Thereinto, taking advantage of the pH gradient, which varies from the physiological pH (7.4, for example, in the systemic circulation) to 6.5−7.2 in tumor tissue, 5.5−6.5 in endosomes, and 4.0−5.0 in lysosomes, two main strategies have been developed: (1) the use of polymers with protonable groups that undergo conformational and/or solubility changes in response to the pH variations; (2) and the design of polymers with acid-sensitive bonds, which results in disassembly of the NPs to promote cargo release once these bonds are cleaved.[22−24] Among various reported pH-sensitive polymers, poly(2-(diisopropylamino) ethyl methacrylate)-(PDPA) possessed ultra pH-sensitivity which varies from hydrophobic to hydrophilic via protonation in the endo/lysosomes for triggering drug release at pH <6.5. However, the problem with the reported PDPA is that more than 20% of loaded drugs were released prematurely in the physiological condition.[28,29]

Herein, the synergetic combination of disulfide cross-linked shell and pH-sensitive PDPA core was expected to be a well strategy to optimize the delivery pattern to be "spatiotemporally pinpointed". As shown in Scheme1, we demonstrate the versatile SCNPs with well-defined structure for tumor targeted drug delivery. By the well-structured fabrication of triblock amphiphilic zwitterionic copolymer RGD-PCB-*b*-PDS-*b*-PDPA (termed as RGD-PCSSD), the SCNPs were cooperatively equipped with pH-sensitive PDPA core for loading anticancer drugs and acid-responsive drug release, disulfide-cross-linked PDS shell for preventing premature drug leakage, zwitterionic PCB corona for stabilizing the SCNPs to obtain prolonged systemic circulation,[25] and RGD ligand for active tumor targeting.[26] These novel SCNPs are expected to be stable with less drug leakage in neutral environment and accumulate predominately in tumor tissue. Upon internalized into cells via receptor-mediated endocytosis, the cross-linked shell would be cleaved by GSH, which presents in abundance within tumor cells. The core would subsequently be disassembled because of the acidic pH (4.0−6.0) to accomplish the "spatiotemporally pinpointed" drug release.

In this study, the reducase and pH dual-sensitive SCNPs were prepared from a well-defined triblock copolymer which was synthesized via reversible addition−fragmentation chain transfer (RAFT) polymerization of carboxybetaine methacrylate (CB), *N*-(2-(2-pyridyl disulde) ethyl methacrylamide (DS), and 2-(diisopropylamino) ethyl methacrylate (DPA). To endow the SCNPs with tumor targeting ability, we conjugated RGD to the PCB segment via amidation reaction.[27] The physicochemical characteristics of the prepared SCNPs, including particle size, micromorphology and drug loading properties were investigated in detail. The pH and redox dual-sensitivity along with their cooperativity were studied systematically by employing the particle size, micromorphology and fluorescence spectra measurement, respectively. The serum stability, storage stability and protein adsorption properties were evaluated. The cellular uptake and intracellular drug release were confirmed by flow cytometry and fluorescence microscope. The in vitro antitumor properties were evaluated by cytotoxicity assay. The in vivo drug distribution and tumor accumulation studies were performed using HepG2 tumor bearing Balb/c nude mice.

Scheme 1. Illustration of the pH and Redox Dual-Sensitivity of the PCSSD/DOX SCNPs; Tumor Targeted Accumulation and Receptor-Mediated Endocytosis; Dual-Sensitivity Cooperatively Triggered Intracellular Drug Release

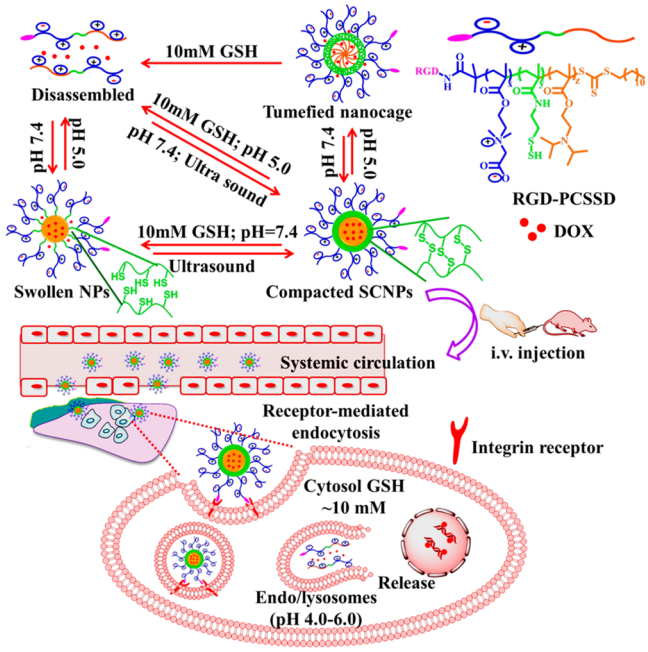

2. EXPERIMENTAL SECTION

2.1. Materials. 2-(Dimethylamino) ethyl methacrylate (DMA), 2-(diisopropylamino) ethyl methacrylate (DPA), *tert*-butyl α-bromoisobutyrate and pyrene were purchased from Sigma-Aldrich. N-(3-(Dimethylamino)propyl)-N′-ethylcarbodiimide hydrochloride (EDC·HCl), trifluoroacetic acid (TFA), 2,2,2-trifluoroethanol (TFE), *N*-Hydroxysuccinimide (NHS), and mercaptoethanol were obtained from Alfa Aesar (Lancashire, UK). Methacryloyl chloride, cysteamine hydrochloride, 2,2′-dithiodipyridine, and dithiothreitol (DTT) were purchased from Aladdin (Shanghai, China). The inhibitors in the DPA monomer was stripped off by passing through a short column packed with neutral alumina. Doxorubicin hydrochloride (DOX·HCl) was purchased from Zhejiang Hisun Pharmaceutical Co. Ltd. Acetonitrile, 2,2-azobis(isobutyronitrile) (AIBN) was obtained from Alfa Aesar (Lancashire, UK). Anhydrous ethyl ether and dimethylformamide were all analytical grade and used as received from Jiangtian company (Tianjin, China). Arg-Gly-Asp (RGD), 3-(4,5-dimethylthiazol-2-yl)-2,5-diphenyl tetrazolium bromide (MTT), bovine serum albumin

Scheme 2. Synthesis Route of the RGD-PCSSD Copolymers

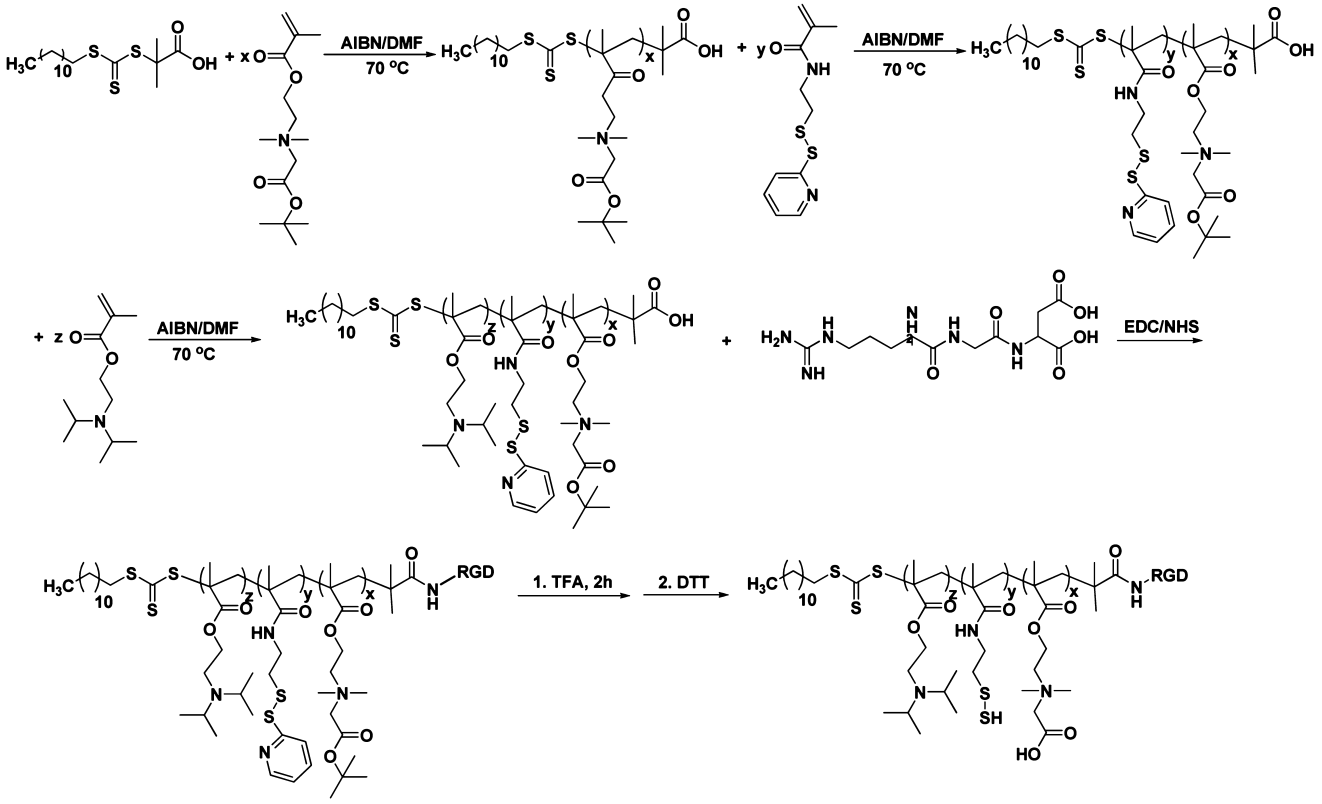

(BSA), fibrinogen (FBG), and 10% fetal bovine serum (FBS) was purchased from Sigma-Aldrich (St. Louis, USA).

2.2. Measurement. Nuclear magnetic resonance instrument (^{1}HNMR) (Varian Unity-Plus INOVA 500) was employed to characterize the structure and composition of the monomer and polymers. The polydispersity index (M_w/M_n) of the copolymers were determined by gel permeation chromatography (GPC), which was equipped with PLgel Oranginc GPC Column (10 um Mixed-B, Org 300 × 7.8 mm) with RI2000 detector. DMF with LiBr (1 g/L) was used as the eluting solvent at a flow rate of 1 mL/min, and polystyrene was used as the standard for calibration. Particle size, size distribution (PDI) of NPs were determined by Zetasizer 3000HS (Malvern Instrument, Inc. Worcestershire, UK) at a wavelength of 633 nm with a constant angle of 173° at room temperature. The micromorphology of blank and DOX-loaded NPs was observed by transmission electron microscopy (TEM, Hitachi H600). The solution of NPs was dropped on the 400-mesh carbon coated grids and excessed sample was removed by filter paper. Then, the sample loaded carbon coated grids were dried at room temperature. The specimens were viewed under the microscope at an accelerating voltage of 100−200.0 kV. The fluorescence spectra were measured by fluorescence spectrophotometer (Varina, FLR Eclipse, Australia).

2.3. Synthesis and Characterization of PCSSD and RGD-PCSSD Copolymers. The synthesis route for the RGD-PCSSD copolymers is shown in Scheme 2. First, the chain transfer agent S-1-dodecyl-S-(α, α'-dimethyl-α''-acetic acid) trithiocarbonate (CTAm) and 2-*tert*-butoxy-N-(2-(methacryloyloxy) ethyl)-N,N-dimethyl-2-oxoethanaminium (CB-tBu) monomer were synthesized as reported.[28,29] The active disulfide bond containing N-[2-(2-pyridyl disulde) ethyl] methacrylamide (DS) monomer was synthesized according to Takeo Yamaguchi's method with some modifications.[30] Briefly, the amino-functionalized pyridyl disulfide molecule 2-(2-pyridyldisulde) ethylammonium chloride was synthesized as reported.[31] Then, the pyridyl disulfide monomer (DS) was synthesized from 2-(2-pyridyldisulde) ethylammonium chloride via amidation reaction. The synthesized 2-(2-pyridyldisulde) ethylammonium chloride (4.45 g, 20 mM) was dispersed in 50 mL anhydrous DCM and solution was added with triethylamine (8.34 mL, 60 mM). After stirring the mixture at 0 °C for 20 mim, methacryloyl chloride (2.33 mL, 24 mM) solution in 30 mL of anhydrous DCM was added dropwise to the 2-(2-pyridyldisulde) ethylammonium chloride dispersion with stirring in an ice bath for 30 min. Then, the reaction progressed for another 24 h at room temperature. The mixture was filtered to remove insoluble substances and then was evaporated at 30 °C. Finally, the product was purified on a silica gel column with an eluting solvent of 20:80 ethyl acetate-hexane. The eluted fraction was monitored by TLC, and the fractions containing the product were combined and evaporated at 30 °C to obtain the product as yellow oil. The successful synthesis of DS was then confirmed by ^{1}HNMR and UV−visible spectrophotometer (TU-1900, China).

Subsequently, the RGD-PCSSD copolymers were obtained with a three-step method. First, the PCB (tBu)-*b*-PDS-*b*-PDPA (PC(tBu)-SSD) triblock copolymer was synthesized by continuous RAFT polymerization, using AIBN as the initiator and CTAm as the chain transfer agent in DMF, which was conducted at 70 °C for 24 h under no oxygen conditions, and then the solution of PC(tBu)SSD copolymers was dialyzed against deioned water and obtained by freeze-drying. In order to endow the PCSSD SCNPs with tumor targeting ability, RGD was conjugated via EDC/NHS chemistry.[27] Briefly, PC(tBu)SSD copolymer was dissolved in 3 mL DMSO and incubated with EDC (5 equiv.) and NHS (10 equiv.) for 30 min, and then the excess amount EDC was quenched by mercaptoethanol. Then, RGD (1.0 equiv) dissolved in 200 μL DMSO was added dropwise and the reaction was continued for another 24 h at RT. The resulting RGD-PC(tBu)SSD solution was dialyzed against pure water for 2 days, and then was lyophilized to obtain the powder of RGD-PC(tBu)SSD copolymer. Finally, the obtained RGD-PC(tBu)SSD copolymers was dissolved in TFA to hydrolyze the tBu ester groups for 2 h. The resulting RGD-PCSSD copolymers were precipitated into ethyl ether, redispersed in a small amount of TFEA, and precipitated in ethyl ether repeatedly. After vacuum-dry, the copolymers were used for preparing the NP formulation. The PCSSD copolymers were obtained by the same method without the conjugation of RGD. The

dx.doi.org/10.1021/am503974y | ACS Appl. Mater. Interfaces 2014, 6, 14631−14643

composition of copolymers was characterized by ^{1}HNMR and UV−vis spectrophotometer.

2.4. Preparation and Characterization of PCSSD SCNPs and PCSSD/DOX SCNPs. In order to prepare the disulfide bond shell cross-linked NPs, the active disulfide bond on PCSSD copolymers should be converted into sulfydryl. Consequently, the transition of pyridyl disulfide to sulfydryl was conducted with the existence of DTT (1.2 equiv.) and the extent of the transition was conveniently monitored by the absorption peak that corresponds to the 2-thiopyridone byproduct.[32]

Subsequently, the PCSSD/DOX SCNPs was prepared via dialysis method. Briefly, 20 mg of PCSSD copolymer and 2 mg of deprotonated DOX were codissolved in 6 mL of DMSO, and then appropriate amount of DTT was added. After being incubated for 30 min, the mixed solution was dialyzed against PBS (0.01M, pH 7.4) for 24 h using a dialysis bag (MWCO: 3500 Da). Then, the solution was subjected to ultrasound for 10 min to form the SCNPs. Finally, the obtained SCNPs solution was filtrated and then subjected to centrifugation at 16000 g using high speed centrifuge followed by washing with deionized water for three times to completely remove the trace amount of organic solvents and by products during the formation of sulfydryl. Blank PCSSD SCNPs NPs were prepared similarly without the addition of DOX.

The DOX-loading content, defined as the weight percentage of DOX in the freeze-dried SCNPs was quantified by UV−visible spectrophotometer. A calibration curve was constructed using different concentrations of DOX (1−50 μg/mL) in DMSO. DLC and DLE were calculated from the following equations:

$$\mathrm{DLC}(\%) = (\text{weight of loaded DOX}/\text{weight of DOX loaded NPs}) \times 100\% \quad (1)$$

$$\mathrm{DLE}(\%) = (\text{weight of loaded DOX}/\text{weight of DOX in feed}) \times 100\% \quad (2)$$

The particle size, size distribution (PDI), morphology of PCSSD SCNPs and PCSSD/DOX SCNPs were measured by Zetasizer and TEM. The serum stability of PCSSD/DOX SCNPs and RGD-PCSSD/DOX SCNPs were studied by mixing solution of the SCNPs with DMEM culture medium containing 10% fetal bovine serum (FBS) at pH 7.4 and the change of particle size was monitored by Zetasizer. The storage stability of PCSSD/DOX SCNPs was conducted by measuring the particle size at pretended time intervals within 2 month.

In addition, the protein adsorption properties of the PCSSD/DOX SCNPs and RGD-PCSSD/DOX SCNPs were evaluated by taking bovine serum albumin (BSA) and fibrinogen (FBG) as the model proteins.[33] The PCSSD/DOX SCNPs and RGD-PCSSD/DOX SCNPs were incubated with BSA or FBG solution in PBS at 7.4, with the concentration of NPs and proteins at 0.18 and 0.25 mg m/L, respectively. After incubation for 24 h at 37 °C, 5 mL of each sample was withdrawn and centrifuged at 10 000 g for 20 min at 20 °C to precipitate the protein adsorbed aggregation. The protein concentration of supernatant was determined using UV−visible spectrophotometer (TU-1900, China). The adsorbed proteins on the aggregate were then calculated against a standard calibration curve.

2.5. Characterization of Cooperativity of pH and Redox Dual-Sensitivity of PCSSD SCNPs. First, the pH and redox dual-sensitivity of PCSSD SCNPs was estimated under conditions simulating environment in vivo by measuring the change of particle size and morphology using Zetasizer and TEM. Briefly, the PCSSD SCNPs suspension (1.0 mg/mL) was divided into four groups, which were adjusted into three different conditions: (i) Na_2HPO_4−citric acid buffer solution (10 mM) with pH varied from 7.4 to 5.0; (ii) Na_2HPO_4−citric acid buffer solution (pH 7.4, 10 mM) containing 20 μM GSH; (iii) Na_2HPO_4−citric acid buffer solution (pH 7.4, 10 mM) containing 10 mM GSH; (iv) Na_2HPO_4−citric acid buffer solution (10 mM) with pH varied from 7.4 to 5.0 containing 10 mM GSH.

Subsequently, the cooperativity of pH and redox dual-sensitivity of SCNPs was verified by not only measuring the pH variation induced change of particle size and morphology, but also taking pyrene (6×10^{-7} mol/L) as the fluorescence probe to monitor the hydration situation of the hydrophobic core all the SCNPs (1 mg/mL, 10 mM PBS) in real time, respectively. The pH values was adjusted by adding 1 N HCl solution dropwise, which was detected with a pH-meter (PH-3C, INESA Scientific Instrument Co., Ltd.). Each sample was equilibrated for 2 h to assess the pH induced change of particle size and fluorescence spectrum.

2.6. In Vitro Drug Release. *2.6.1. Influence of Cross-Linking Density on the Controlled-Release Behavior.* First, the influence of cross-linking density on the controlled drug release behavior of PCSSD/DOX SCNPs was investigated. To obtain the drug release profile, 5 mL PCD/DOX NPs, $PCSS_5D$/DOX SCNPs and $PCSS_{10}D$/DOX SCNPs (1 mg/mL) were sealed in a dialysis bag (MWCO: 3500) and incubated in 40 mL of buffer solutions at 37 °C under oscillation with the pH value maintaining at 7.4 and 5.0, respectively. At scheduled time intervals, 5 mL of release medium was withdrawn for testing and replaced with an equal volume of fresh medium. The amount of drug released was detected by UV−visible spectrophotometry.

2.6.2. pH and Redox Dual-Sensitivity Triggered Drug Release Behavior. Second, the pH and redox dual-sensitivity cooperatively triggered drug release of PCSSD/DOX SCNPs was verified. The drug release research was carried out in PBS of different pH values of 7.4, 6.5, and 5.0 containing 10 mM GSH. To obtain the drug release profile, we sealed 5 mL of PCSSD/DOX SCNPs (1 mg/mL) in a dialysis bag (MWCO: 3500) and incubated in 40 mL of release medium at 37 °C under oscillation. At scheduled time intervals, 5 mL of release medium was withdrawn for testing and replaced with an equal volume of fresh medium.

2.7. Cellular Uptake and Intracellular Drug Release Studies. *2.7.1. Cell Culture.* HepG2 cells were maintained in Hyclone Ham's/F12 medium. All media were supplemented with 10% heat-inactivated fetal bovine serum (FBS), penicillin (100 U/mL), and streptomycin (100 U/mL). All cell lines were maintained at 37 °C and 5% CO_2 in a humidified atmosphere.

2.7.2. Cellular Uptake Studies. HepG2 cells were seeded in 24 well plates at a density of 2×10^5 cells per well in 0.5 mL of DMEM medium and incubated at 37 °C in 5% CO_2 humidified atmosphere for 24 h. The original medium was discarded and washed twice with PBS. Fresh DMEM medium containing free DOX, PCD/DOX NPs, PCSSD/DOX SCNPs, and RGD-PCSSD/DOX SCNPs was then added. The cells were incubated for 4 h at 37 °C, and then washed three times with cold PBS and harvested by trypsin treatment. The harvested cells were suspended in PBS and centrifuged at 1000 g for 5 min at 4 °C. The supernatants were discarded and the cell pellets were washed with PBS to remove the background fluorescence in the medium. After two cycles of washing and centrifugation, cells were resuspended with 200 μL of PBS for analyses using FACS Calibur flow cytometer (BD Biosciences, USA) with argon laser excitation at 488 nm (Becton Dickinson) and fluorescence (FL3) was detected. Cells treated with PBS were used as control.

2.7.3. Intracellular Drug Release Studies. HepG2 cells were seeded in 24-well plates with 2×10^4 cells per well in 0.5 mL of DMEM culture medium and incubated under standard cell culture conditions. Then, cells were washed twice with PBS and fresh medium was added with free DOX, PCD/DOX NPs, PCSSD/DOX SCNPs and RGD-PCSSD/DOX SCNPs. After 4 h incubation, cells were washed twice with ice-cold PBS and fixed with fresh 4% paraformaldehyde for 15 min at room temperature. The intracellular release behaviors of RGD-PCSSD/DOX SCNPs were further conducted after incubation for 6 and 8 h. The cells were counterstained 4,6-diamidino-2-phenylindole (DAPI) for the cell nucleus with an excitation of 405 nm sequentially following the standard protocol of the manufacturer before imaged on fluorescence microscopy (Leica AF 6500), and the fluorescence of DOX were observed under an excitation of 543 nm.

2.8. In Vitro Antitumor Efficiency Study. The cytotoxicity of blank and DOX loaded PCD NPs, PCSSD SCNPs, and RGD-PCSSD NPs against HeLa and HepG 2 cells was evaluated by MTT assay. HeLa and HepG 2 cells were seeded in 96-well plates at 5000 cells per

well in 100 μL of DMEM culture medium and incubated under standard cell culture conditions. The culture medium was replaced with 100 μL of fresh medium containing the NPs and SCNPs at pH 7.4. After treatment for 48 h, the medium was replaced by 100 μL fresh DMEM medium followed by addition of 25 μL of MTT stock solution (5 mg/mL in PBS). After incubation for an additional 2 h, 100 μL of the extraction buffer (20% SDS in 50% DMF, pH 4.7) was added to the wells and incubated overnight at 37 °C. The absorbance of the solution was measured at 570 nm using a microplate reader. The results were expressed as a percentage of the absorbance of the blank control.

2.9. In Vivo Drug Distribution and Tumor Accumulation Studies. The Balb/c nude mice (female, 6−8 weeks old) bearing HepG2 tumor model was used for drug accumulation studies. When the mean volume of tumor reached 200 mm^3, free DOX, PCD/DOX NPs, PCSSD/DOX SCNPs and RGD-PCSSD/DOX SCNPs were administrated intravenously into the tail vein at an equivalent dose of 5 mg/kg. At scheduled time intervals, the mice were sacrificed, and then the major organs and tumor were harvested. These obtained organs were examined by the Kodak IS in vivo FX imaging system.

To further quantify the drug accumulation amount in tumor tissues, the excised tumor tissues were washed with cold saline and dried by filter paper and then weighed. The obtained tumors were homogenized in borate buffer solution (10 mM, pH 9.0). In terms of the $PCSS_{10}D$/DOX SCNPs and RGD-$PCSS_{10}D$/DOX SCNPs groups, 20 mM of DTT was added to the borate buffer solution. Subsequently, 300 μL tissue homogenate was taken out and extracted with 500 μL chloroform/isopropanol (6:1, v/v) by vortex for three times. After centrifugation (12000 g, 15 min), the organic phase was separated and dried by vacuum drying oven. The residue was dissolved in 0.5 mL of mobile phase and followed by filtered with ultrafiltration membrane (220 nm). Eventually, the filtrate was collected for HPLC analysis. The amount of DOX was determined by HPLC (Lab Alliance Model 201) with a Hypersil ODS-2 (250 mm × 4.6 mm, 5 μm) C18 column and the detection wavelength was set at 480 nm. The mobile phase was composed of acetonitrile and water (50:50, v/v) with pH 2.74 adjusted by $HClO_4$. The injection volume was 20 μL and the flow rate of mobile phase was 1.0 mL/min. To obtain the standard curve for DOX, the samples were prepared by adding free DOX to the tumor tissue homogenate from untreated mice. The linear detection range was 0.1−30 μg/mL.

All animals were obtained from the Vital River Laboratory Animal Technology Co., Ltd. (Beijing, China) and housed individually in plastic cages in a controlled environment with free access to food and water. All animal experiments were performed in accordance with the People's Republic of China national standard (GB/T 16886.6−1997).

3. RESULTS AND DISCUSSION

3.1. Synthesis and Characterization of PCSSD and RGD-PCSSD Copolymers. The PCSSD copolymers were synthesized via RAFT polymerization followed by selective hydrolysis of the *tert*-butyl groups of CB-tBu units. As shown in Scheme 2, the chain transfer agent CTAm and CB-tBu monomer were synthesized according to previous report and characterized with ^{1}HNMR (shown in Figure S1 in the Supporting Information).[28,29] The DS monomer with active disulfide bond was synthesized according to Takeo Yamaguchi's method with some modifications.[30] Then, the PC(tBu)SSD copolymer was synthesized by RAFT polymerization, using AIBN as the initiator and CTAm as the chain transfer agent in DMF under no oxygen conditions. Subsequently, the hydrolysis of the tBu ester groups was rapidly accomplished in TFA within 2 h to obtain the final PCSSD copolymers.

The chemical structures and compositions of PCSSD copolymers were determined by ^{1}HNMR and GPC characterization. The details of obtained polymers are listed in Table 1. As shown in Figure 1B, all characteristic signals of CTAm, PCB

Table 1. Chemical Structure and Composition of PCSSD Copolymers

	composition (/unit)				
samples	CB[a]	DS[a]	DPA[a]	M_n (Da)[a]	M_w/M_n[b]
PCD	25	0	25	10 312	1.44
$PCSS_5D$	25	5	25	11 583	1.36
$PCSS_{10}D$	25	10	25	12 856	1.57

[a]Calculated by ^{1}HNMR spectra. [b]Determined by GPC.

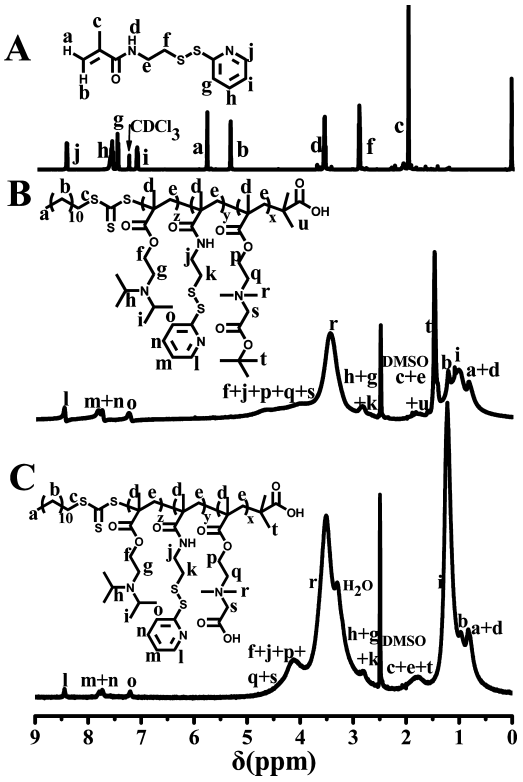

Figure 1. ^{1}H NMR spectra of (A) DS monomer, (B) PCB(tBu)SSD, and (C) PCSSD copolymers.

(tBu), PDS and PDPA segments could be seen clearly. After hydrolysis reaction, the characteristic resonance of $-C(CH_3)_3$ in the CB-tBu unit at 1.48 ppm disappeared, indicating that PCB (tBu)SSD copolymers were successfully converted to PCSSD copolymers. There were ten repeated methylene ($-CH_2-$) on the CTAm molecular. Therefore, the repeating units of PCB, PDS and PDPA could be calculated by comparing the integral areas of characteristic peaks of the DPA unit at 1.02 ppm ($-$-N$-$CH$-(CH_3)_2$), DS unit at 8.48 ppm ($-CH{=}N-$) and the CB unit at 3.45 ppm ($-N-(CH_3)_2$) with the known CTAm unit ($-CH_2-$) at 1.22 ppm. The composition and molecular weights calculated by ^{1}HNMR agreed well with the feeding ratio. In addition, the PCSSD copolymers were also analyzed by UV−vis spectrum, since the pyridyl disulfide had characteristic absorption at 281 nm and RGD had characteristic absorption at 260 nm. As shown clearly in Figure S2 in the Supporting Information, the obtained RGD-PCSSD copolymer had the same ultraviolet absorption in comparation with the DS monomer and RGD, indicating the successful incorporation of active pyridyl disulfide and RGD.[32] Furthermore, GPC was employed to determine the molecular weight distribution (M_w/M_n) of the obtained PCD and PCSSD polymers and the results were summarized in Table 1. The

Table 2. Characterization of PCSSD NPs and PCSSD/DOX SCNPs

	blank NPs		DOX-loaded NPs			
sample	size (nm)[a]	PDI[a]	size (nm)[a]	PDI[a]	DLC (%)[b]	DLE (%)[b]
PCD	135 ± 3.5	0.11 ± 0.05	143 ± 3.4	0.15 ± 0.02	5.5 ± 0.3	55 ± 0.3
$PCSS_5D$	142 ± 3.8	0.12 ± 0.02	153 ± 2.7	0.12 ± 0.01	5.6 ± 0.2	56 ± 0.2
$PCSS_{10}D$	153 ± 3.2	0.13 ± 0.04	160 ± 5.2	0.13 ± 0.02	5.4 ± 0.4	54 ± 0.4

[a]Determined by Zetasizer. [b]Determined by UV−vis spectra. The feeding ratio of DOX was 10%.

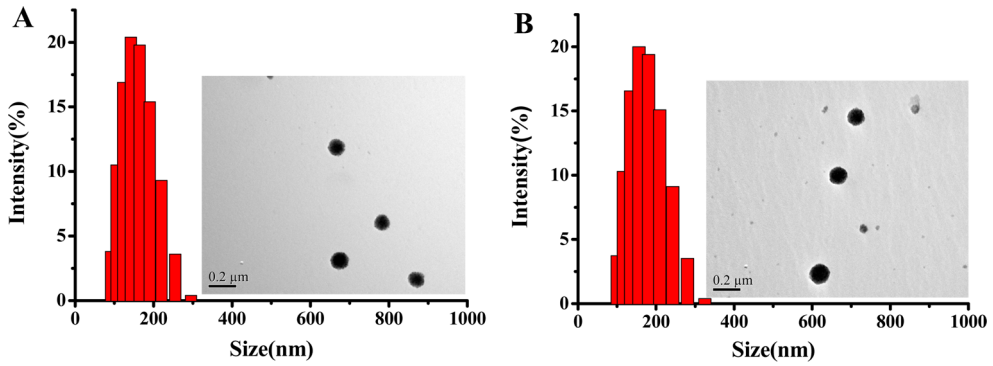

Figure 2. (A) Size distribution and morphology of $PCSS_{10}D$ SCNPs; (B) $PCSS_{10}D$/DOX SCNPs.

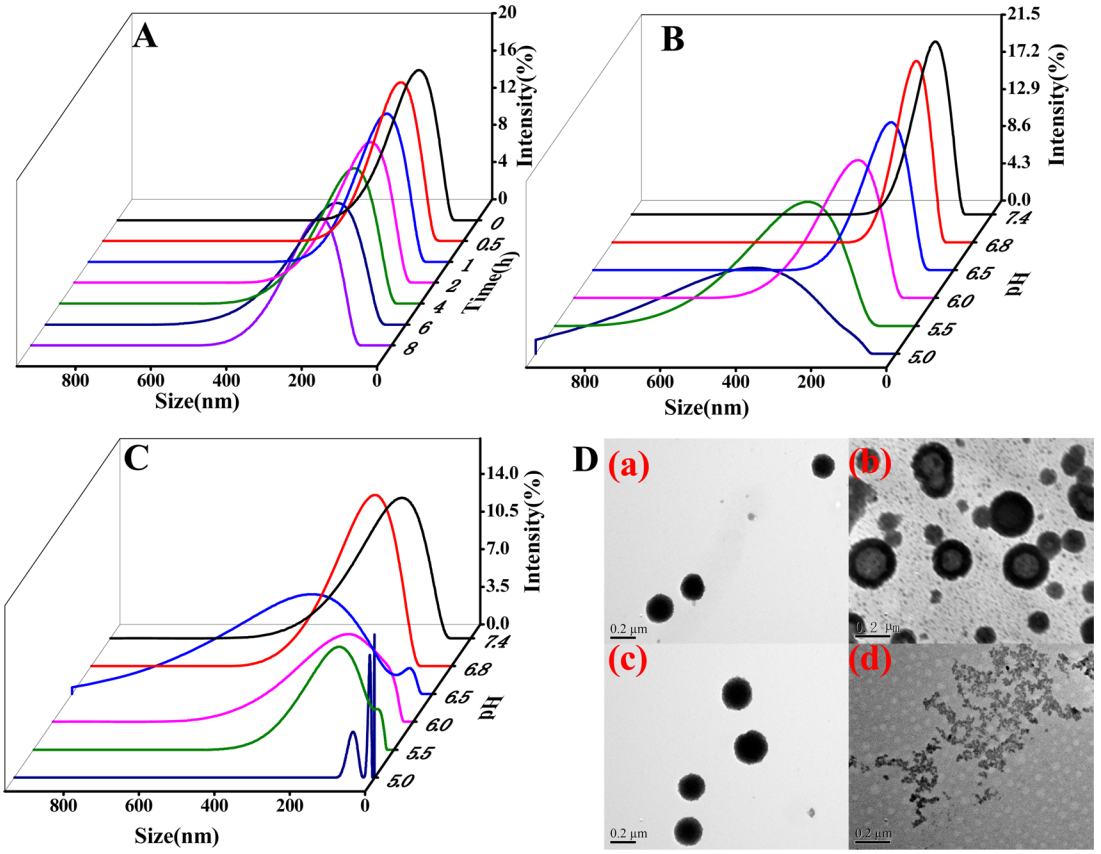

Figure 3. Change of particle size of $PCSS_{10}D$ SCNPs triggered by (A) GSH (10 mM), (B) pH variation, (C) GSH (10 mM) and pH combined action; (D) morphology of $PCSS_{10}D$ SCNPs: (a) pH 7.4, (b) pH 5.0, and (c) pH 7.4 with GSH (10 mM); (d) pH 5.0 with GSH (10 mM).

results showed narrow distribution of all the obtained PCD polymers, indicating the well-controlled polymerization process and effective purification methods (shown in Figure S3 in the Supporting Information).

3.2. Preparation and Characterization of PCSSD and PCSSD/DOX SCNPs. In order to form the disulfide bond cross-linked shell, the active disulfide bond on PCSSD copolymers should be converted into sulfydryl. Consequently, the transition of pyridyl disulfide to sulfydryl was conducted with the existence of DTT (1.2 equiv) and the extent of the transition was monitored by UV absorbance spectra of the 2-thiopyridone byproduct, which was substantially different from

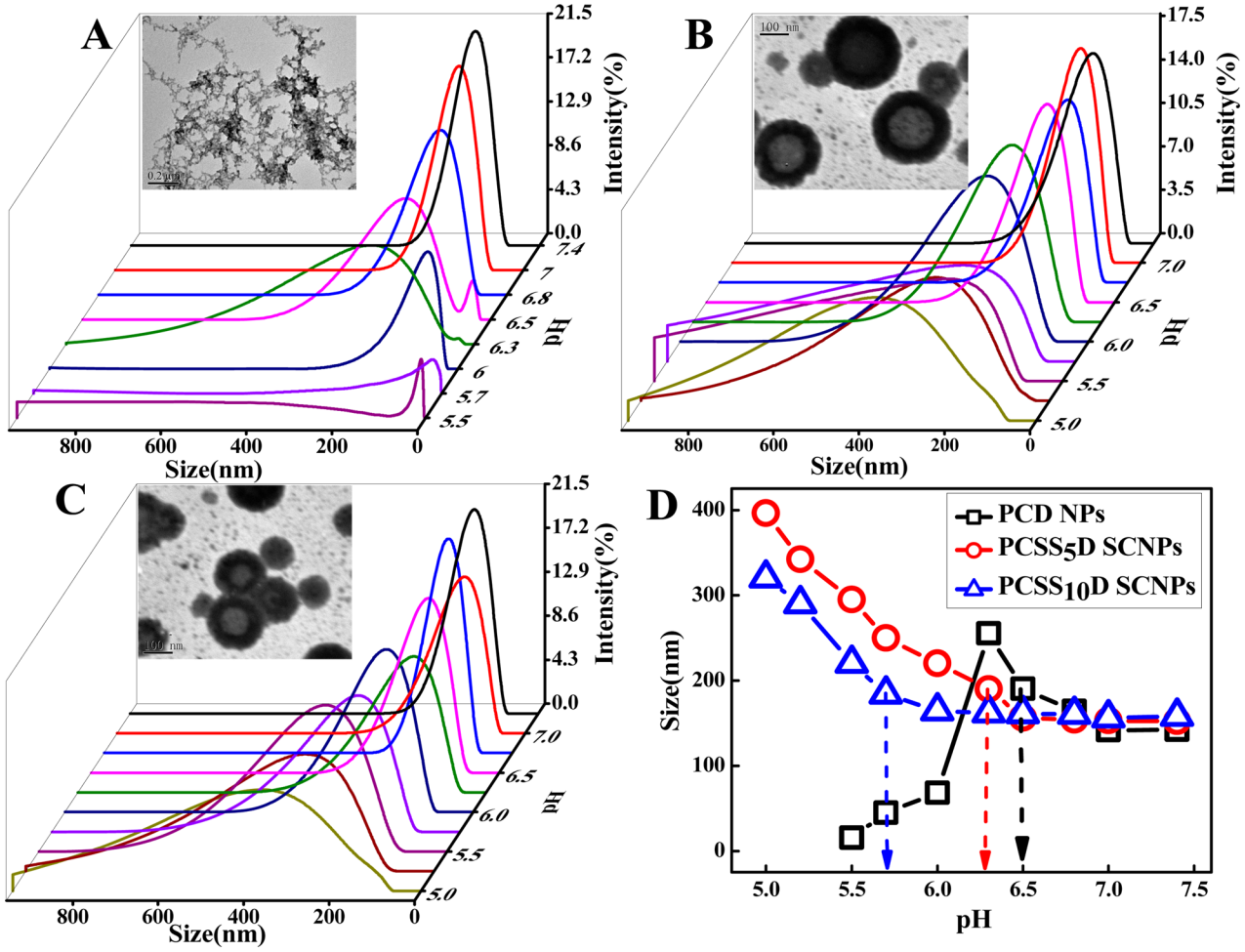

Figure 4. Particle size change and morphology at pH 5.0 of (A) PCD NPs, (B) $PCSS_5D$ SCNPs, and (C) $PCSS_{10}D$ SCNPs; (D) summary of particle size change as a function of pH.

that of PCSSD copolymers and DS monomer.[32] As shown in Figure S4 in the Supporting Information, after the solution was incubated with DTT for 5 min, the UV absorbance spectra of the PCSSD copolymer solution changed dramatically. However, after incubation for 10 min, the absorbance spectra of the PCSSD copolymer solution remained unchanged, indicating that the pyridyl disulfide bond was converted to sulfydryl completely.

Then, the PCSSD and PCSSD/DOX SCNPs were prepared via dialysis method followed by ultrasound treatment to facilitate the formation of cross-linked shell. The particle size, PDI and micromorphology of the SCNPs were examined by Zetasizer and TEM. Then, the DLC and DLE were determined by UV−vis spectra. The results are listed in Table 2. As can be seen clearly in Figure 2, the size distribution was narrow and the particles were all spherical in shape with obvious core−shell structure. Importantly, the particle size of all DOX loaded NPs were less than 200 nm, which were expected to accumulate into the tumor tissues effectively taking advantage of the EPR effect.[5,8,9,34] In addition, all the prepared DOX-loaded NPs represented excellent serum stability within 72 h, which was mainly due to the fact that the hydrophilic PCB block with anionic and cationic groups at the microscopic range could form hydration layer via electrostatic interactions.[25,35,36] Importantly, the storage stability of DOX-loaded NPs was significantly enhanced via shell-cross-linking (shown in Figure S5 in the Supporting Information). In addition, the shell cross-linking had no obvious influence on the drug loading capacity.

As shown in Figure S6 in the Supporting Information, the conjugation of RGD had no obvious influence on the serum stability and protein adsorption property of the $PCSS_{10}D$ SCNPs, indicating that the RGD-functionalization had negligible influence on the nonfouling property of PCB segment. Significantly, the NPs with considerable serum stability and low protein adsorption property would be expected to exhibit prolonged systemic circulation time in vivo.[37]

3.3. Cooperativity of pH and Redox Dual-Sensitivity of PCSSD SCNPs and PCSSD/DOX SCNPs. The pH and redox dual sensitivity of $PCSS_{10}D$ SCNPs were studied by Zetasizer and TEM measurements. Since the diisopropyl groups of DPA units were completely deprotonated at pH 7.4, the $PCSS_{10}D$ copolymer could assemble a micelle structure with a compact core of hydrophobic PDPA segments in aqueous solution at pH 7.4. Figure 3Da explained the small particle size with well-defined core−shell structure of the $PCSS_{10}D$ SCNPs. As shown in Figure 3A and Dc, upon adding GSH (10 mM) at pH 7.4, which mimicked the concentration of GSH inside tumor cells, integrated particles with very slight expansion were observed as a function of time, which was mainly due to the extension of the hydrophilic segments with the shedding of the cross-linked interlayer. In addition, the

dx.doi.org/10.1021/am503974y | ACS Appl. Mater. Interfaces 2014, 6, 14631−14643

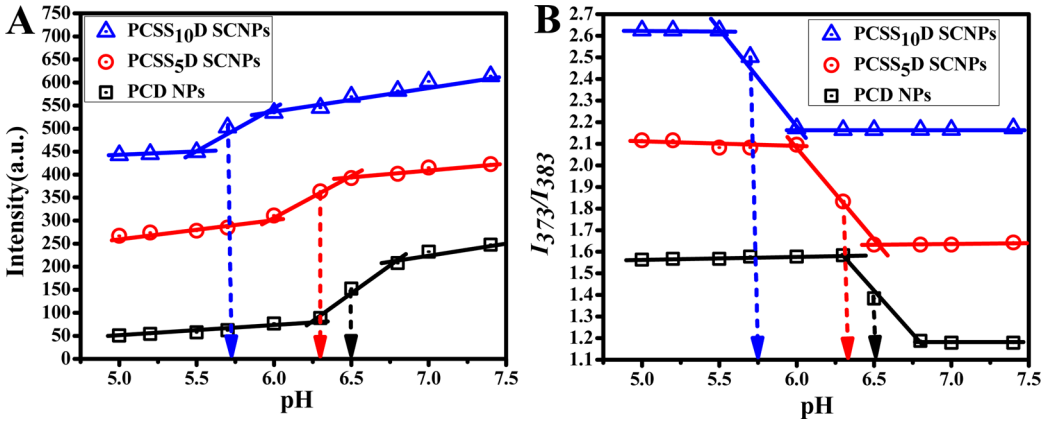

Figure 5. (A) the fluorescence intensity at 393 nm and (B) intensity ratios of I_{373}/I_{383} of pyrene in PCD NPs, $PCSS_5D$ SCNPs, and $PCSS_{10}D$ SCNPs solutions as a function of pH, respectively.

concentration of GSH outside tumor cells had negligible influence on the $PCSS_{10}D$ SCNPs (shown in Figure S7 in the Supporting Information). As shown in Figure 3B, integrated particles with very slight expansion (from 163.4 to 183.7 nm) was also observed with the pH of the solution varied from 7.4 to 6.0, whereas a significant increase in the particle size and PDI (from 354 to 183.7 nm; 0.183 to 0.35) was observed upon further lowering the pH to 5.0. However, it had been reported that the ultra pH-sensitive PDPA block revealed a sharp transition from hydrophobic to hydrophilic at pH 6.5 within a narrow interval of less than 0.25,[38] indicating that drug release would partially occurred in the tumor matrix (pH 6.5−6.8). Herein, it was inferred that, by the shell cross-linked design, the protonation of the PDPA core was significantly restricted and the integral structure of the nanoparticles was remained outside of tumor cells. Meanwhile, the premature drug release during the systemic circulation and in the tumor matrix could be reduced.

Subsequently, to verify the above inference, we studied the cooperativity of cross-linked shell and pH-sensitive core of the PCSSD SCNPs by measuring the change of particle size and morphology under different pH conditions with different cross-linking density. As illustrated in Figure 4A, there was an obvious increase in the particle size for the PCD NPs without cross-linked shell when the pH was decreased to 6.5, which was mainly due to the partial protonation of the PDPA blocks affording the electrostatic repulsion among positively charged amine groups and consequently hindering the dense packing of the hydrophobic core of the NPs. Upon further decreasing the pH to 5.0, the PCD NPs were hardly detected because the PDPA blocks became completely protonated and the PCD copolymers were dissolved completely. Consequently, the morphology of PCD NPs at pH 5.0 was detected by TEM measurements which represented as random polymeric aggregates. However, for the $PCSS_5D$ SCNPs and $PCSS_{10}D$ SCNPs, delayed and weakened change of particle size was observed at pH 6.3 and 5.7 respectively, which was lower than that of PCD NPs (shown in Figure 4B−D). Therefore, it was verified the above inference that the cross-linked shell had significant restriction on the partially protonated core of PCSSD SCNPs against expansion and disruption, which increased with the increase of cross-linking density. In other words, the pK_a* value could be teamed as the balanced point between the core expansion force induced by protonation and the shell cross-linking induced restrictive effect (shown in Figure 4D).

Meanwhile, pyrene was employed as the fluorescence probe to monitor the real-time hydration situation of the hydrophobic core, due to its highly sensitivity to the change of polarity.[39] The fluorescence emission spectrum was shown in Figure S8 in the Supporting Information. The change in fluorescence intensity at characteristic peak 393 nm and intensity ratio of I_{373}/I_{383} was clearly pH-dependent (shown in Figure 5). As can be seen, the variation trend of fluorescence intensity and intensity ratio of I_{373}/I_{383} was consistent well with the change of particle size. Dramatic decrease of fluorescence intensity and increase of intensity ratio of I_{373}/I_{383} was observed upon the pK_a* was reached, corresponding to the significant change of the surrounding polarity encountered with pyrene. Upon further lowering the pH, the PDPA blocks were totally positively charged and hence became hydrophilic and swelling, which resulted in the further decrease of fluorescence intensity and increase of intensity ratio of I_{373}/I_{383}. Therefore, it was further verified the cooperativity of cross-linked shell and ultra pH-sensitive core.

Eventually, when GSH (10 mM) was added to the solution, the $PCSS_{10}D$ SCNPs was turned into a highly "tumefied" nanocage at pH 6.5, since the partially protonated $PCSS_{10}D$ SCNPs core was able to expand upon unpacking the tight enclosure of the cross-linked shell (Figure 3C). Upon further lowering the pH to 5.0, disassembly of the $PCSS_{10}D$ SCNPs was detected by zetasizer, which indicated that the disulfide cross-linking was destroyed and the polymer chains were completely dissolved. In addition, drying the solution led to the formation of random polymeric aggregates (Figure 3Dd). Namely, once the PCSSD SCNPs located inside the tumor cells encountering with higher concentrated GSH and lower pH, rapid dissociation of SCNPs could be induced by shell de-cross-linking accompanying with disassembly of PDPA core, which would facilitate boost intracellular drug release. As to the $PCSS_{10}D$ SCNPs, the cross-linked density provided a suitable pK_a* value for "spatiotemporally pinpointed" intracellular drug delivery.

3.4. In Vitro and Intracellular Drug Release. Understandably, disulfide bond cross-linked shell has demonstrated great potential for tuning encapsulation stability and specific drug release. However, the influence of cross-linking degree on the drug release behavior and its mechanism has not been studied systematically in peer works.[14,15,18,40] In this study, the

drug release of PCSSD SCNPs with different cross-linking density was conducted. As shown in Figure 6, the release rate

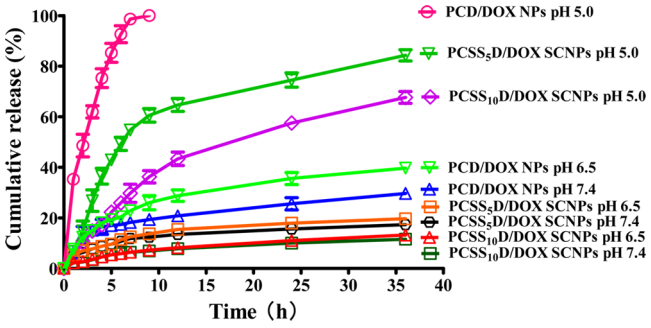

Figure 6. In vitro drug release of PCSSD/DOX SCNPs with different cross-linking density at different pH.

was clearly density-dependent. The higher the cross-linking density was, the lower the drug release rate was. At pH 7.4, about 20% of loaded drugs were released within 12 h for PCD/DOX NPs. However, it was reduced to 14% and 8% for the $PCSS_5D/DOX$ SCNPs and $PCSS_{10}D/DOX$ SCNPs within the same time, respectively. Significantly, at pH 6.5, the drug release was also confined efficiently to less than 20% within 12h for $PCSS_{10}D/DOX$ SCNPs, while approximately 30% was released for PCD/DOX NPs. The above results indicated that $PCSS_{10}D/DOX$ SCNPs with cross-linked shell could reduce drug losing before the NPs were internalized by tumor cells, which was consistent with the influence of cross-linked shell on the structure of SCNPs. Despite that, the drug release of $PCSS_{10}D/DOX$ SCNPs was still retarded at pH 5.0, when fast drug release was expected. However, the most obvious and spectacular microenvironments of cancer cells were not only the intrinsic pH gradient, which varied from 7.4 in the systemic circulation to 4.0−6.0 in the endo/lysosomal compartments, but also the concentration of GSH which varied from 2 to 20 μM in the body fluids and normal extracellular matrices to 2−10 mM in the cytosol within tumor cells.[20] Hence, the $PCSS_{10}D/DOX$ SCNPs with better controlled released behavior were employed in the following pH and redox dual-sensitivity triggered drug release studies, which were inves-

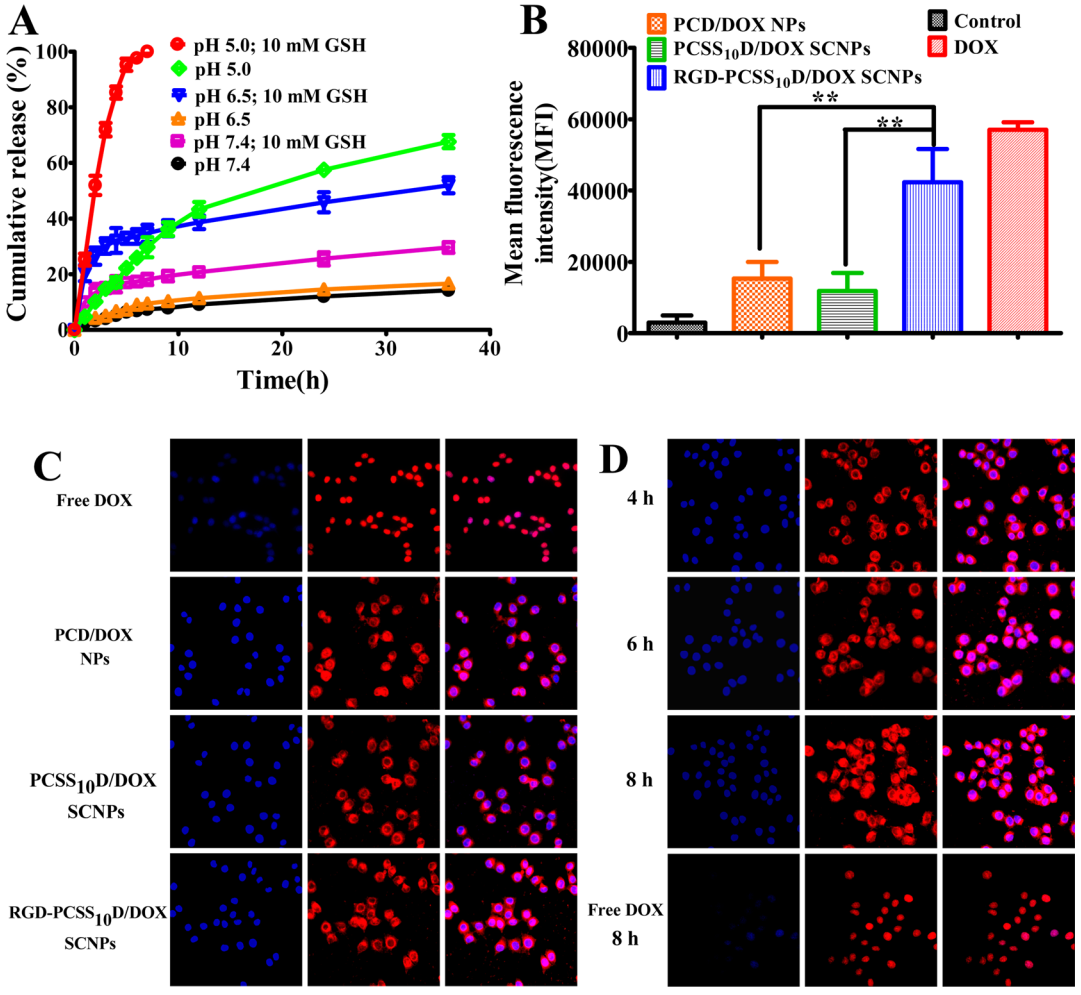

Figure 7. (A) In vitro drug release of $PCSS_{10}D/DOX$ SCNPs at 37 °C in PBS at different pH and redox conditions. (B) Quantitive measurement of the mean fluorescence intensity after incubated with free DOX, PCD/DOX NPs, $PCSS_{10}D/DOX$ SCNPs and RGD-$PCSS_{10}D/DOX$ SCNPs for 4 h via flow cytometry (blank cells as the control, $*p < 0.05$, $**p < 0.01$ in comparasion with RGD-$PCSS_{10}D/DOX$ SCNPs). (C) Fluorescence microscopy images of HepG2 cells after incubated with free DOX, $PCSS_{10}D/DOX$ SCNPs, and RGD-$PCSS_{10}D/DOX$ SCNPs for 4 h. (D) Fluorescence microscopy images of HepG2 cells after incubated with RGD-$PCSS_{10}D/DOX$ SCNPs for 4, 6, and 8 h, respectively. For each panel, images from left to right show cell nuclei stained by DAPI (blue), DOX fluorescence in cells (red) and overlays of two images.

dx.doi.org/10.1021/am503974y | ACS Appl. Mater. Interfaces 2014, 6, 14631−14643

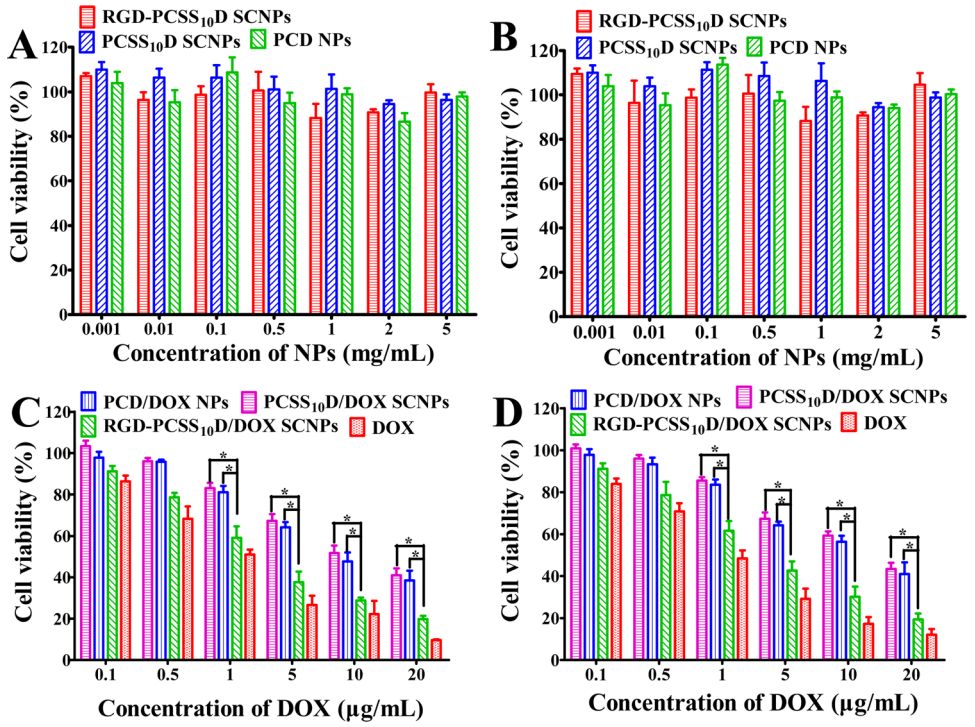

Figure 8. (A) Viability of HepG2 and (B) HeLa cells after incubation with PCD NPs, $PCSS_{10}D$ SCNPs and RGD-$PCSS_{10}D$ SCNPs for 48 h; (C) viability of HepG2 and (D) HeLa cells after incubation with free DOX, PCD/DOX NPs, $PCSS_{10}D$/DOX SCNPs and RGD-$PCSS_{10}D$/DOX SCNPs for 48 h. (*$p < 0.05$ in comparation with PCD-2/DOX NPs). Error bars represent the standard deviation ($n = 6$).

tigated systematically under conditions that simulated the gradient in vivo.

As shown in Figure 7A, evident acceleration of DOX release was observed upon either adjusting the pH to 5.0 or adding 10 mM GSH, however, the most rapid release was detected when dual stimulation were applied synchronously. Upon dual-stimulation, the loaded DOX was released completely within 5 h, which was similar to the PCD/DOX NPs at pH 5.0, indicating that the defense of the cross-linked shell was removed in the intracellular environment of tumor cells. The dual-stimuli triggered DOX release behavior could be well-explained by the above results of structural transitions of $PCSS_{10}D$ SCNPs and fluorescence spectra of $PCSS_{10}D$/DOX SCNPs induced by the coordinated dual-sensitivity (shown in Figures 3 and 6).

Subsequently, the cellular uptake was evaluated by flow cytometry. As shown in Figure 7B, the fluorescence intensity of RGD-$PCSS_{10}D$/DOX SCNPs treated group was significantly higher than that of PCD/DOX NPs and $PCSS_{10}D$/DOX SCNPs ($p < 0.01$). The lower level of DOX delivered by PCD/DOX NPs and $PCSS_{10}D$/DOX SCNPs was mainly attributed to the nonfouling property of the PCB segments on the surface of the SCNPs, which hindered the endocytosis of NPs.[29,33,41] Significantly, the conjugation of RGD ligand enhanced the endocytosis of the $PCSS_{10}D$/DOX SCNPs, since the RGD targeting ligand could specifically bind to the $\alpha_v\beta_3$ integrin receptor highly expressed at the surface of malignant cells.[26,42−44] Therefore, without affecting the nonfouling property of PCB segments, the conjugation of RGD ligand could efficiently overcome the dilemma of PCB in endocytosis to provide enhanced specific tumor cell internalization of the NPs. As shown in Figure 7C, the result of fluorescence microscopy observation was consistent with the result of cellular uptake studies.

To further evaluate the intracellular drug release, RGD-$PCSS_{10}D$/DOX SCNPs were incubated with HepG2 cells for another 6 and 8 h, followed by observation using fluorescence microscopy (shown in Figure 7D). Obviously, DOX fluorescence was mainly located around the cell nucleus in cytoplasm after incubation for 4 h. More importantly, certain increase of fluorescence intensity of DOX was observed in cell nucleus with prolonging the incubation time to 6 and 8 h, as DOX is known to exert drug effects via intercalation with DNA and inhibition of macromolecular biosynthesis.[45−47] The rapid release of DOX from the RGD-$PCSS_{10}D$ SCNPs intracellularly was consistent with the result of drug release obtained in PBS, indicating that DOX can be released effectively within tumor cells triggered by acid microenvironment in endo/lysosomal compartment and GSH in the cytoplasm, and then be delivered into cell nucleus.

3.5. In Vitro Cytotoxicity Assay. Further anticancer evaluation verified the importance of the pH and reduction dual-sensitivity cotriggered rapid release of DOX. As shown in Figure 8A, B, The blank NPs and SCNPs showed very low cytotoxicity even at fairly high concentrations up to 5 mg/mL, indicating the well cell compatibility of the prepared materials. In addition, the cytotoxicity of RGD-$PCSS_{10}D$/DOX SCNPs was significantly higher than PCD/DOX NPs and $PCSS_{10}D$/DOX SCNPs, which was mainly due to the fact that the nonfouling PCB segment hindered the endocytosis of NPs. This result was in consistent with the cellular uptake studies. As summarized in Table 3, the IC_{50} values were 3.45 and 2.82 μg/mL for RGD-$PCSS_{10}D$/DOX SCNPs on HepG2 and HeLa cells, respectively. In terms of $PCSS_{10}D$/DOX SCNPs, the IC_{50} values were 15.83 and 11.91 μg/mL correspondingly.

3.6. In Vivo Drug Distribution and Tumor Accumulation Studies. In the above studies, all the prepared NPs and SCNPs exhibited excellent serum stability and especially low

Table 3. IC_{50} Value of Free DOX and NPs Formulations

sample	IC_{50}(μg/mL)	
	HepG2 cell	HeLa cell
free DOX	0.99	1.15
PCD/DOX NPs	14.12	9.34
$PCSS_{10}D$/DOX SCNPs	15.83	11.91
RGD-$PCSS_{10}D$/DOX SCNPs	3.45	2.82

protein adsorption properties, which would be expected to realize prolonged blood circulation time in vivo.[37,48,49] However, the drug-loaded NPs must complete a sophisticated journey from the injection site to the tumor tissue where they have to overcome tremendous challenges.[4] Namely, protein adsorption of the NPs in the blood is much more sophisticated than that from model protein, as plasma is full of multiple proteins, whose adsorption is regarded as a selective and competitive process.[37,50] To evaluate the accumulation of DOX in tumor tissue, we injected free DOX, PCD/DOX NPs, $PCSS_{10}D$/DOX SCNPs, and RGD-$PCSS_{10}D$/DOX SCNPs intravenously into nude mice bearing HepG2 tumor xenografts. The intrinsic fluorescence of DOX enabled direct tracking of the distribution of DOX loaded NPs during the ex vivo imaging of organs of interest. As shown in Figure 9A, it could be seen clearly that both NPs formulations enhanced the accumulation of DOX in the tumor tissue in comparison with free DOX, which was in consistent with the previous report that NPs with similar small sizes (30−200 nm) accumulated preferentially in tumors through the enhanced permeability and retention (EPR) effect and at the reticuloendothelial sites such as liver.[8,9,50] In addition, as shown in Figure 9B, significantly stronger fluorescence of DOX was detected in the tumor tissue with the administration of all the NPs formulations after injected for 5 h. Subsequently, the quantitative analyzation of DOX concentration in tumor tissues is shown in Figure 9C. The concentration of DOX in tumor tissues with administration of RGD-$PCSS_{10}D$/DOX SCNPs showed a 1.16, 1.23, and 1.73 times higher level than $PCSS_{10}D$/DOX SCNPs, PCD/DOX NPs and free DOX after administrations for 5 h, respectively. Particularly, the proportion was increased to 1.46, 1.75, and 2.87 fold post-injection for 24 h. Normally, NPs with zwitterionic polymer surfaces are expected to accumulate equally into tumor interstitials through the EPR effect, however, the $PCSS_{10}D$/DOX SCNPs showed higher DOX accumulation amount in comparation with the non-cross-linked PCD/DOX NPs, which are supportive of reduced drug release from shell cross-linked NPs in blood circulation. In addition, the enhanced accumulation of RGD-$PCSS_{10}D$/DOX SCNPs could be attributed to the functionalization of RGD, which was able to specifically bind to the $\alpha_v\beta_3$ integrin receptor highly expressed on the surface of proliferating neovascular endothelial cells and malignant cells in tumor and subsequently promote the internalization into tumor cells.[43,51] As reported, NPs that could not be internalized by tumor cells were easily eliminated from the tumor site because of the high interstitial fluid pressure (IFP).[52,53] Consequently, this result could be explained as the cooperation of the PCB for prolonged systemic circulation, RGD for active tumor targeting and cellular uptake, cross-linked shell for reduced premature drug release, which facilitated the improvement of tumor accumulation and retention of DOX.

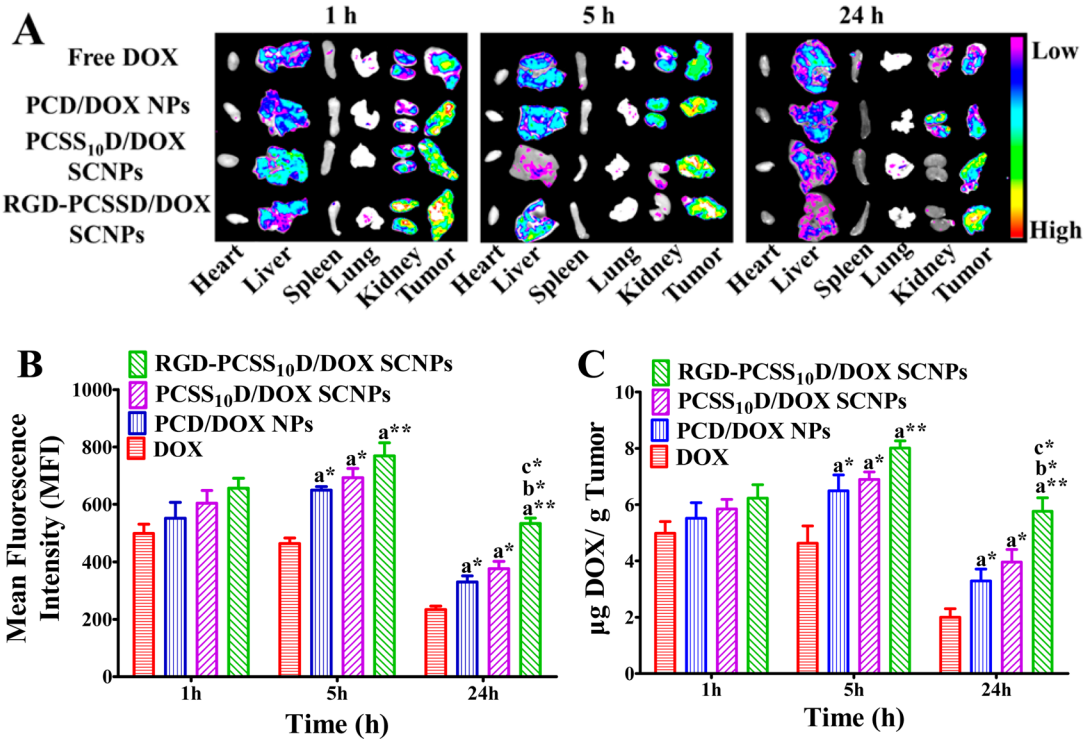

Figure 9. (A) Fluorescence images of major organs and tumor after administration of different formulations at scheduled time intervals. (B) Mean fluorescence intensities of DOX in tumor tissues. (C) Quantitative analyses the concentration of DOX in tumor tissues. (*p < 0.05, **p < 0.01, a = in comparation with free DOX, b = in comparation with PCD/DOX NPs, c = in comparation with $PCSS_{10}D$/DOX SCNPs). (The data were expressed as mean ± SD, n = 3.)

4. CONCLUSION

In this study, multifunctional SCNPs were fabricated via one-step assembly of well-defined triblock zwitterionic PCSSD copolymers, which were synthesized via reversible additive fragment transfer (RAFT) polymerization and followed by functionalization with RGD. The RGD-PCSSD SCNPs were able to cooperatively combine the functions of ultra pH-sensitive PDPA core for efficient loading and pH-triggered release of anticancer drugs, disulfide-cross-linked PDS shell for preventing premature drug release, zwitterionic PCB corona for stabilizing the SCNPs and acquiring prolonged systemic circulation, and RGD ligand for active tumor targeting and receptor-mediated endocytosis. The results of in vitro and in vivo evaluation showed that the cooperativity was accomplished as to enable the RGD-PCSSD/DOX SCNPs to complete the sophisticated journey from the initial injection site to the tumor tissue and "spatiotemporally pinpointed" drug release intracellularly. Consequently, this well-constructed multifunctional RGD-PCSSD/DOX SCNPs, which represented the cooperative design view, showed great potential for the development of novel nanocarriers in tumor targeted drug delivery.

■ ASSOCIATED CONTENT

Supporting Information

Electronic Supporting Information (ESI) available: ^{1}HNMR spectra of chain transfer agent CTAm and CB-tBu monomer; UV−visible spectra of DS monomer, RGD-PCSS$_{10}$D, PCSSD copolymers and RGD; GPC of PCSSD copolymers; reduction-sensitivity of PCSSD copolymers; serum stability and storage stability of PCSSD/DOX SCNPs; serum stability and protein adsorption property of PCSSD/DOX SCNPs and RGD-PCSSD/DOX SCNPs; change of particle size of PCSS$_{10}$D SCNPs triggered by GSH (20 μM) at pH 7.4; The fluorescence emission spectrum of pyrene in (A) PCD NPs, (B) PCSS$_5$D SCNPs and (C) PCSS$_{10}$D SCNPs solutions as a function of pH. This material is available free of charge via the Internet at http://pubs.acs.org.

■ AUTHOR INFORMATION

Corresponding Authors

*E-mail: ajdong@tju.edu.cn.
*E-mail: lewis78@163.com.

Author Contributions

‡P.H. and J.L. contributed equally to this work.

Notes

The authors declare no competing financial interest.

■ ACKNOWLEDGMENTS

This project was supported by the National Natural Science Foundation of China (31271073, 81301309, and 81171371).

■ REFERENCES

(1) Zhang, Y.; Chan, H. F.; Leong, K. W. Advanced Materials and Processing for Drug Delivery: The Past and the Future. *Adv. Drug Delivery Rev.* **2012**, *65*, 104−120.
(2) Mitragotri, S.; Lahann, J. Materials for Drug Delivery: Innovative Solutions to Address Complex Biological Hurdles. *Adv. Mater.* **2012**, *24*, 3717−3723.
(3) Elsabahy, M.; Wooley, K. L. Design of Polymeric Nanoparticles for Biomedical Delivery Applications. *Chem. Soc. Rev.* **2012**, *41*, 2545−2556.
(4) Nichols, J. W.; Bae, Y. H. Odyssey of a Cancer Nanoparticle: From Injection Site to Site of Action. *Nano Today* **2012**, *7*, 606−618.
(5) Allen, T. M.; Cullis, P. R. Drug Delivery Systems: Entering the Mainstream. *Science* **2004**, *303*, 1818−1822.
(6) Nicolas, J.; Mura, S.; Brambilla, D.; Mackiewicz, N.; Couvreur, P. Design, Functionalization Strategies and Biomedical Applications of Targeted Biodegradable/Biocompatible Polymer-Based Nanocarriers for Drug Delivery. *Chem. Soc. Rev.* **2013**, *42*, 1147−1235.
(7) Vallet-Regi, M.; Ruiz-Hernandez, E.; Gonzalez, B.; Baeza, A. Design of Smart Nanomaterials for Drug and Gene Delivery. *J. Biomater. Tissue Eng.* **2011**, *1*, 6−29.
(8) Fang, J.; Nakamura, H.; Maeda, H. The EPR effect: Unique Features of Tumor Blood Vessels for Drug Delivery, Factors Involved, and Limitations and Augmentation of the Effect. *Adv. Drug Delivery Rev.* **2011**, *63*, 136−151.
(9) Maeda, H.; Nakamura, H.; Fang, J. The EPR Effect for Macromolecular Drug Delivery to Solid Tumors: Improvement of Tumor Uptake, Lowering of Systemic Toxicity, and Distinct Tumor Imaging in vivo. *Adv. Drug Delivery Rev.* **2013**, *65*, 71−9.
(10) Kataoka, K.; Harada, A.; Nagasaki, Y. Block Copolymer Micelles for Drug Delivery: Design, Characterization and Biological Significance. *Adv. Drug Delivery Rev.* **2001**, *47*, 113−131.
(11) Shuai, X. T.; Ai, H.; Nasongkla, N.; Kim, S.; Gao, J. M. Micellar Carriers Based on Block Copolymers of Poly(epsilon-caprolactone) and Poly(ethylene glycol) for Doxorubicin Delivery. *J. Controlled Release* **2004**, *98*, 415−426.
(12) Chang, L.; Deng, L.; Wang, W.; Lv, Z.; Hu, F.; Dong, A.; Zhang, J. Poly(ethyleneglycol)-b-Poly(epsilon-caprolactone-co-gamma-hydroxyl-epsil on-caprolactone) Bearing Pendant Hydroxyl Groups as Nanocarriers for Doxorubicin Delivery. *Biomacromolecules* **2012**, *13*, 3301−3310.
(13) Read, E. S.; Armes, S. P. Recent Advances in Shell Cross-Linked Micelles. *Chem. Commun.* **2007**, 3021−3035.
(14) Liu, S. Y.; Weaver, J. V. M; Tang, Y. Q.; Billingham, N. C.; Armes, S. P.; Tribe, K. Synthesis of Shell Cross-Linked Micelles with pH-Responsive Cores Using ABC Triblock Copolymers. *Macromolecules* **2002**, *35*, 6121−6131.
(15) Dai, J.; Lin, S. D.; Cheng, D.; Zou, S. Y.; Shuai, X. T. Interlayer-Crosslinked Micelle with Partially Hydrated Core Showing Reduction and pH Dual Sensitivity for Pinpointed Intracellular Drug Release. *Angew. Chem., Int. Ed.* **2011**, *50*, 9404−9408.
(16) Sun, H.; Guo, B.; Cheng, R.; Meng, F.; Liu, H.; Zhong, Z. Biodegradable Micelles with Sheddable Poly(ethylene glycol) Shells for Triggered Intracellular Release of Doxorubicin. *Biomaterials* **2009**, *30*, 6358−6366.
(17) Chan, N.; Khorsand, B.; Aleksanian, S.; Oh, J. K. A Dual Location Stimuli-Responsive Degradation Strategy of Block Copolymer Nanocarriers for Accelerated Release. *Chem. Commun.* **2013**, *49*, 7534−7536.
(18) Koo, A. N.; Lee, H. J.; Kim, S. E.; Chang, J. H.; Park, C.; Kim, C.; Park, J. H.; Lee, S. C. Disulfide-Cross-Linked PEG-Poly(amino acid)s Copolymer Micelles For Glutathione-Mediated Intracellular Drug Delivery. *Chem. Commun.* **2008**, 6570−6572.
(19) Hu, X.; Li, H.; Luo, S.; Liu, T.; Jiang, Y.; Liu, S. Thiol and pH Dual-Responsive Dynamic Covalent Shell Cross-Llinked Micelles for Triggered Release of Chemotherapeutic Drugs. *Polym. Chem.* **2013**, *4*, 695−706.
(20) Meng, F.; Cheng, R.; Deng, C.; Zhong, Z. Intracellular Drug Release Nanosystems. *Mater. Today* **2012**, *15*, 436−442.
(21) Zhuang, J.; Gordon, M. R.; Ventura, J.; Li, L.; Thayumanavan, S. Multi-Stimuli Responsive Macromolecules and Their Assemblies. *Chem. Soc. Rev.* **2013**, *42*, 7421−7435.
(22) Du, J.-Z.; Du, X.-J.; Mao, C.-Q.; Wang, J. Tailor-Made Dual pH-Sensitive Polymer-Doxorubicin Nanoparticles for Efficient Anticancer Drug Delivery. *J. Am. Chem. Soc.* **2011**, *133*, 17560−17563.
(23) Du, Y.; Chen, W.; Zheng, M.; Meng, F.; Zhong, Z. pH-Sensitive Degradable Chimaeric Polymersomes for the Intracellular Release of Doxorubicin Hydrochloride. *Biomaterials* **2012**, *33*, 7291−7299.
(24) Guan, X.; Li, Y.; Jiao, Z.; Chen, J.; Guo, Z.; Tian, H.; Chen, X. A pH-Sensitive Charge-Conversion System for Doxorubicin Delivery. *Acta Biomater.* **2013**, *9*, 7672−7678.

(25) Cao, Z.; Jiang, S. Super-hydrophilic Zwitterionic Poly-(carboxybetaine) and Amphiphilic Non-Ionic Poly(ethylene glycol) for Stealth Nanoparticles. *Nano Today* **2012**, *7*, 404−413.
(26) Brooks, P. C.; Clark, R. A.; Cheresh, D. A. Requirement of Vascular Integrin alpha$_v$ beta$_3$ for Angiogenesis. *Science* **1994**, *264*, 569−71.
(27) Cao, Z.; Yu, Q.; Xue, H.; Cheng, G.; Jiang, S. Nanoparticles for Drug Delivery Prepared from Amphiphilic PLGA Zwitterionic Block Copolymers with Sharp Contrast in Polarity between Two Blocks. *Angew. Chem., Int. Ed.* **2010**, *49*, 3771−3776.
(28) Lai, J. T.; Filla, D.; Shea, R. Functional Polymers from Novel Carboxyl-Terminated Trithiocarbonates as Highly Efficient RAFT Agents. *Macromolecules* **2002**, *35*, 6754−6756.
(29) Jiang, S.; Cao, Z. Ultralow-Fouling, Functionalizable, and Hydrolyzable Zwitterionic Materials and Their Derivatives for Biological Applications. *Adv. Mater.* **2010**, *22*, 920−932.
(30) Sugawara, Y.; Tamaki, T.; Ohashi, H.; Yamaguchi, T. Control of the Poly(N-isopropylacrylamide) Phase Transition via a Single Strand-Double Strand Transformation of Conjugated DNA. *Soft Matter* **2013**, *9*, 3331−3340.
(31) Ebright, Y. W.; Chen, Y.; Kim, Y.; Ebright, R. H. S-[2-(4-A zidosalicylamido) Ethylthio]-2-Thiopyridine: Radioiodinatable, Cleavable, Photoactivatible Cross-Linking Agent. *Bioconjugate Chem.* **1996**, *7*, 380−384.
(32) Wang, L. X.; Kristensen, J.; Ruffner, D. E. Delivery of Antisense Oligonucleotides Using HPMA Polymer: Synthesis of a Thiol Polymer and Its Conjugation to Water-Soluble Molecules. *Bioconjugate Chem.* **1998**, *9*, 749−757.
(33) Yuan, Y. Y.; Mao, C. Q.; Du, X. J.; Du, J. Z.; Wang, F.; Wang, J. Surface Charge Switchable Nanoparticles Based on Zwitterionic Polymer for Enhanced Drug Delivery to Tumor. *Adv. Mater.* **2012**, *24*, 5476−5480.
(34) Duncan, R. The Dawning Era of Polymer Therapeutics. *Nat. Rev. Drug Discovery* **2003**, *2*, 347−360.
(35) Cheng, G.; Li, G.; Xue, H.; Chen, S.; Bryers, J. D.; Jiang, S. Zwitterionic Carboxybetaine Polymer Surfaces and Their Resistance to Long-term Biofilm Formation. *Biomaterials* **2009**, *30*, 5234−5240.
(36) Zhang, L.; Xue, H.; Cao, Z.; Keefe, A.; Wang, J.; Jiang, S. Multifunctional and Degradable Zwitterionic Nanogels for Targeted Delivery, Enhanced MR Imaging, Reduction-Sensitive Drug Release, and Renal Clearance. *Biomaterials* **2011**, *32*, 4604−4608.
(37) Salmaso, S.; Caliceti, P. Stealth Properties to Improve Therapeutic Eefficacy of Drug Nanocarriers. *J. Drug Delivery* **2013**, *2013*, 374252−374252.
(38) Zhou, K.; Wang, Y.; Huang, X.; Luby-Phelps, K.; Sumer, B. D.; Gao, J. Tunable, Ultrasensitive pH-Responsive Nanoparticles Targeting Specific Endocytic Organelles in Living Cells. *Angew. Chem., Int. Ed.* **2011**, *50*, 6109−6114.
(39) Wilhelm, M.; Zhao, C. L.; Wang, Y.; Xu, R.; Winnik, M. A.; Mura, J. L.; Riess, G.; Croucher, M. D. Poly(styrene-ethylene oxide) Block Copolymer Micelle Formation in Water: a Fluorescence Probe Study. *Macromolecules* **1991**, *24*, 1033−1040.
(40) Yang, T. F.; Chen, C. N.; Chen, M. C.; Lai, C. H.; Liang, H. F.; Sung, H. W. Shell-Crosslinked Pluronic L121 Micelles as a Drug Delivery Vehicle. *Biomaterials* **2007**, *28*, 725−734.
(41) White, A. D.; Nowinski, A. K.; Huang, W.; Keefe, A. J.; Sun, F.; Jiang, S. Decoding Nonspecific Interactions from Nature. *Chem. Sci.* **2012**, *3*, 3488−3494.
(42) Quan, C. Y.; Chen, J. X.; Wang, H. Y.; Li, C.; Chang, C.; Zhang, X. Z.; Zhuo, R. X. Core-Shell Nanosized Assemblies Mediated by the alpha-beta Cyclodextrin Dimer with a Tumor-Triggered Targeting Property. *ACS Nano* **2010**, *4*, 4211−4219.
(43) Zhen, Z.; Tang, W.; Chen, H.; Lin, X.; Todd, T.; Wang, G.; Cowger, T.; Chen, X.; Xie, J. RGD-Modified Apoferritin Nanoparticles for Efficient Drug Delivery to Tumors. *ACS Nano* **2013**, *7*, 4830−4837.
(44) Han, H. D.; Mangala, L. S.; Lee, J. W.; Shahzad, M. M. K.; Kim, H. S.; Shen, D.; Nam, E. J.; Mora, E. M.; Stone, R. L.; Lu, C.; Lee, S. J.; Roh, J. W.; Nick, A. M.; Lopez-Berestein, G.; Sood, A. K. Targeted Gene Silencing Using RGD-Labeled Chitosan Nanoparticles. *Clin. Cancer Res.* **2010**, *16*, 3910−3922.
(45) Tewey, K. M.; Rowe, T. C.; Yang, L.; Halligan, B. D.; Liu, L. F. Adriamycin-Induced DNA Damage Mediated by Mammalian DNA Topoisomerase II. *Science* **1984**, *226*, 466−8.
(46) Gewirtz, D. A. A Critical Evaluation of the Mechanisms of Action Proposed for the Antitumor Effects of the Anthracycline Antibiotics Adriamycin and Daunorubicin. *Biochem. Pharmacol.* **1999**, *57*, 727−741.
(47) Minotti, G.; Menna, P.; Salvatorelli, E.; Cairo, G.; Gianni, L. Anthracyclines: Molecular Advances and Pharmacologic Developments in Antitumor Activity and Cardiotoxicity. *Pharmacol. Rev.* **2004**, *56*, 185−229.
(48) Moghimi, S. M.; Hunter, A. C.; Murray, J. C. Long-Circulating and Target-Specific Nanoparticles: Theory to Practice. *Pharmacol. Rev.* **2001**, *53*, 283−318.
(49) Brannon-Peppas, L.; Blanchette, J. O. Nanoparticle and Targeted Systems for Cancer Therapy. *Adv. Drug Delivery Rev.* **2004**, *56*, 1649−1659.
(50) Stark, W. J. Nanoparticles in Biological Systems. *Angew. Chem., Int. Ed.* **2011**, *50*, 1242−1258.
(51) Bartczak, D.; Sanchez-Elsner, T.; Louafi, F.; Millar, T. M.; Kanaras, A. G. Receptor-Mediated Interactions between Colloidal Gold Nanoparticles and Human Umbilical Vein Endothelial Cells. *Small* **2011**, *7*, 388−394.
(52) Heldin, C. H.; Rubin, K.; Pietras, K.; Ostman, A. High Interstitial fluid Pressure - An Obstacle in Cancer Therapy. *Nat. Rev. Cancer* **2004**, *4*, 806−813.
(53) Holback, H.; Yeo, Y. Intratumoral Drug Delivery with Nanoparticulate Carriers. *Pharm. Res.* **2011**, *28*, 1819−1830.